Effects of film thickness and mismatch strains on magnetoelectric coupling in vertical heteroepitaxial nanocomposite thin films

H. T. Chen, L. Hong, and A. K. Soh[a)]
Department of Mechanical Engineering, The University of Hong Kong, Hong Kong, People's Republic of China

(Received 18 February 2011; accepted 26 March 2011; published online 3 May 2011)

The phase field model is adopted to study the magnetoelectric coupling effects in vertical heteroepitaxial nanocomposite thin films. Both the lateral epitaxial strains between the film and the substrate and the vertical epitaxial strains between the ferroelectric and ferromagnetic phases are accounted for in the model devised. The effects of the film thickness on the magnetic-field-induced electric polarization (MIEP) are investigated. The results obtained show that the MIEP is strongly dependent on the film thickness, as well as on the vertical and lateral epitaxial strains. © *2011 American Institute of Physics*. [doi:10.1063/1.3583599]

I. INTRODUCTION

Multiferroic materials[1–3] that combine two or more of the ferroic properties ferroelectricity, ferromagnetism, and ferroelasticity have attracted considerable interest for their potential applications as multifunctional devices.[4–6] Magnetoelectric (ME) coupling effects, i.e., the variation of the polarization induced by an applied magnetic field or of the magnetization induced by an applied electric field, can be realized in multiferroics with the coexistence of ferroelectricity and ferromagnetism. Weak ME effects at low temperatures have been observed in some single-phase materials,[7,8] and this limits their practical applications considerably. Comparatively, composite multiferroics[9,10] can produce much larger ME coupling effects due to the incorporation of magnetostrictive and electrostrictive effects. Although large ME coupling effects have been observed in bulk bilayer multiferroics, the ME coupling effects that exist in artificially assembled bilayer epitaxial nanocomposite thin films are weak due to the clamping effects from the substrate.[11] However, the reported enhancement of elastic coupling resulting from the larger interfacial area between the two phases in a vertical heteroepitaxial nanocomposite thin film with ferromagnetic (FM) nanopillars embedded in a ferroelectric (FE) matrix,[12] in which the clamping effect from the substrate is reduced, has triggered great enthusiasm for the study of ME effects in such nanocomposite thin films. Compared with bulk composite multiferroics, nanocomposite thin films possess more degrees of freedom in tuning the ME coupling effects due to their three-dimensional epitaxial properties. Some theoretical works have been carried out in order to study the ME coupling effects in such multiferroics; for example, the magnetic-field-induced electric polarization (MIEP) was studied[13] using the Green's function technique, and the influence of the elastic stresses induced by the FE–FM and film–substrate interfaces on the ME coupling was investigated using the time-dependent Ginzburg–Landau equation.[14] Because the stress states were only approximately determined in those works, they are unable to provide a good understanding of the behavior of complex nanostructures. The phase field approach is a promising method for the study of ME coupling effects, as not only the ferroelectric and ferromagnetic domain states can be determined during the evolution process but also the long-range elastic interactions in a multiferroic. However, in the phase field study carried out by Zhang *et al.*,[15] only the lateral epitaxial misfit strains were accounted for, not the corresponding vertical strains, which have been observed experimentally as the domineering strains in films of relatively large thicknesses (say, more than 20 nm).[16] As the large lattice mismatch between the FE and FM phases cannot be fully relaxed by the embedded pillars with small diameters in the nanocomposite film, significant vertical epitaxial strains would exist and would affect the ME coupling in the film. Therefore, both the lateral and vertical epitaxial misfit strains should be taken into account in phase field modeling.

In the present study, a three-dimensional (3D) phase field model is devised in which both the lateral and vertical epitaxial misfit strains are included in the strain state. The effects of the thickness on the magnetic-field-induced electric polarization will be investigated.

II. PHASE FIELD MODELING

In the present study, $BaTiO_3$–$CoFe_2O_4$ vertical heteroepitaxial nanostructure multiferroic thin films are investigated; a schematic diagram of these films is depicted in Fig. 1(a). Note

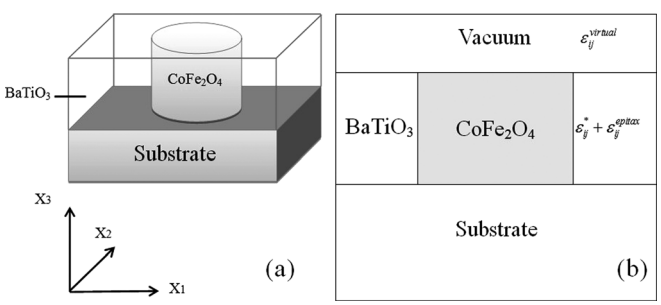

FIG. 1. (a) 3D schematic illustration of a vertical heteroepitaxial nanocomposite film in which $CoFe_2O_4$ nanopillars are embedded in a $BaTiO_3$ matrix. (b) Cross-section of the simulation system along the $x_1 - x_3$ plane.

a)Author to whom correspondence should be addressed. Electronic mail: aksoh@hkucc.hku.hk. FAX: +852-58585415.

that a circular nanopillar was selected for the investigation in view of the experimental work carried out by Zheng *et al.*,[12] in which the multiferroic composite fabricated was composed of nearly circular $CoFe_2O_4$ nanopillars embedded in a $BaTiO_3$ matrix. Three field parameters are introduced to characterize the total free energy of the nanocomposite system: a local polarization field $\mathbf{P}=(P_1, P_2, P_3)$; a local magnetization field $\mathbf{M}=M_s\,\mathbf{m}=M_s\,(m_1, m_2, m_3)$, where M_s and $\mathbf{m}$ denote the saturation magnetization and the unit magnetization vector, respectively; and an order parameter η, which describes the spatial distribution of the FE and FM phases in the nanocomposite film, where $\eta=1$ and 0 represent the FM and FE phases, respectively. The total free energy of the system is given by

$$F = \int_V \left[(1-\eta)f_p + \eta f_m + f_{\text{elas}}\right] dV, \tag{1}$$

where f_p represents the free energy in the FE phase, including the ferroelectric bulk free energy, ferroelectric domain wall energy, and electrostatic energy, which can be expressed as

$$\begin{aligned} f_p =& \alpha_1\left(P_1^2+P_2^2+P_3^2\right)+\alpha_{11}\left(P_1^4+P_2^4+P_3^4\right)+\alpha_{12}\left(P_1^2P_2^2+P_2^2P_3^2+P_3^2P_1^2\right)\\ &+\alpha_{111}\left(P_1^6+P_2^6+P_3^6\right)+\alpha_{112}\left[P_1^4\left(P_2^2+P_3^2\right)+P_2^4\left(P_1^2+P_3^2\right)+P_3^4\left(P_1^2+P_2^2\right)\right]\\ &+\alpha_{123}\left(P_1^2+P_2^2+P_3^2\right)+\alpha_{1111}\left(P_1^8+P_2^8+P_3^8\right)+\alpha_{1122}\left(P_1^4P_2^4+P_2^4P_3^4+P_3^4P_1^4\right)\\ &+\alpha_{1112}\left[P_1^6\left(P_2^2+P_3^2\right)+P_2^6\left(P_1^2+P_3^2\right)+P_3^6\left(P_1^2+P_2^2\right)\right]\\ &+\alpha_{1123}\left(P_1^4P_2^2P_3^2+P_2^4P_3^2P_1^2+P_3^4P_1^2P_2^2\right)+\frac{1}{2}G_{11}\left(P_{1,1}^2+P_{2,2}^2+P_{3,3}^2\right)\\ &+G_{12}\left(P_{1,1}P_{2,2}+P_{2,2}P_{3,3}+P_{3,3}P_{1,1}\right)+\frac{1}{2}G_{44}\left[\left(P_{1,2}+P_{2,1}\right)^2+\left(P_{2,3}+P_{3,2}\right)^2+\left(P_{1,3}+P_{3,1}\right)^2\right]\\ &+\frac{1}{2}G'_{44}\left[\left(P_{1,2}-P_{2,1}\right)^2+\left(P_{2,3}-P_{3,2}\right)^2+\left(P_{1,3}-P_{3,1}\right)^2\right]-\mathbf{E}_{\text{dip}}\cdot\mathbf{P}, \end{aligned} \tag{2}$$

where α_1, α_{11}, α_{12}, α_{111}, α_{112}, α_{123}, α_{1111}, α_{1122}, α_{1112}, and α_{1123} are the phenomenological Landau expansion coefficients; G_{11}, G_{12}, G_{44}, and G'_{44} are the gradient energy coefficients; and $\mathbf{E}_{\text{dip}}$ is the electric field generated by the long-range dipole–dipole interaction that can be established in Fourier space. The commas in the subscripts denote spatial differentiation.

The ferromagnetic energy term f_m, which includes the magnetocrystalline anisotropy energy, magnetic exchange energy, magnetostatic energy, and external magnetic field energy, can be expressed as

$$\begin{aligned} f_m =& K_1\left(m_1^2m_2^2+m_1^2m_3^2+m_2^2m_3^2\right)+K_2m_1^2m_2^2m_3^2\\ &+A\left(m_{1,1}^2+m_{1,2}^2+m_{1,3}^2+m_{2,1}^2+m_{2,2}^2+m_{2,3}^2+m_{3,1}^2\right.\\ &\left.+m_{3,2}^2+m_{3,3}^2\right)-\frac{1}{2}\mu_0M_s\mathbf{H}_d\cdot\mathbf{m}-\mu_0M_s\mathbf{H}_{\text{ex}}\cdot\mathbf{m}, \end{aligned} \tag{3}$$

where K_1 and K_2 are the anisotropy constants, and A, μ_0, M_s, $\mathbf{H}_d$, and $\mathbf{H}_{\text{ex}}$ denote the exchange stiffness constant, permeability of vacuum, saturation magnetization, demagnetization field, and exterior magnetic field, respectively.

The elastic energy f_{elas} can be expressed as

$$f_{\text{elas}} = \frac{1}{2}c_{ijkl}e_{if}e_{kl} = \frac{1}{2}c_{ijkl}\left(\varepsilon_{ij}-\varepsilon_{ij}^0\right)\left(\varepsilon_{kl}-\varepsilon_{kl}^0\right), \tag{4}$$

where c_{ijkl}, e_{ij}, ε_{ij}, and ${\varepsilon_{ij}}^0$ represent the elastic stiffness tensor, elastic strain, total strain, and stress-free strain, respectively. With reference to Fig. 1(b), the elastic energy in the heterogeneous film/substrate bilayer system is calculated by reducing the system to an elastic homogeneous system with an appropriately chosen effective stress-free strain ε_{ij}^0.[17] Thus, the effective stress-free strain in this nanocomposite film is the sum of the strain ε_{ij}^* related to the electrostrictive/magnetostrictive effect, the epitaxial misfit strain $\varepsilon_{ij}^{\text{epitax}}$, and the virtual stress-free strain $\varepsilon_{ij}^{\text{virtual}}$, that is,

$$\varepsilon_{ij}^0 = \varepsilon_{ij}^* + \varepsilon_{ij}^{\text{epitax}} + \varepsilon_{ij}^{\text{virtual}}. \tag{5}$$

The electrostrictive/magnetostrictive related stress-free strain is given by

$$\varepsilon_{ij}^* = \begin{cases} \eta\left[\frac{3}{2}\lambda_{100}\left(m_im_j-\frac{1}{3}\right)\right]+(1-\eta)\left(Q_{ijkl}P_kP_l\right) & (i=j)\\ \eta\left(\frac{3}{2}\lambda_{111}m_im_j\right)+(1-\eta)Q_{ijkl}P_kP_l & (i\neq j), \end{cases} \tag{6}$$

where Q_{ijkl} is the electrostrictive coefficient; i, j, k, $l=1$, 2, 3; and λ_{100} and λ_{111} are the magnetostrictive constants.

The epitaxial misfit strain $\varepsilon_{ij}^{\text{epitax}}$, which arises from the lateral lattice mismatch between the film and the substrate and the vertical lattice mismatch between the FE and FM phases, can be expressed as

$$\varepsilon_{ij}^{\text{epitax}}\begin{bmatrix} \varepsilon_{11}^t & 0 & 0\\ 0 & \varepsilon_{22}^t & 0\\ 0 & 0 & \varepsilon_{33}^t \end{bmatrix}, \tag{7}$$

in which the in-plane epitaxial misfit strains ${\varepsilon_{11}}^t = {\varepsilon_{22}}^t = (1-\eta)\varepsilon_{11}^p + \eta\varepsilon_{11}^m$ are described as a function of the film thickness[18] as follows:

$$\varepsilon_{11}^p = \varepsilon_{22}^p = 1-\frac{\left(1-\varepsilon_{11}^{p0}\right)}{1-\varepsilon_{11}^{p0}\left(1-h_c^p/h\right)}, \tag{8a}$$

$$\varepsilon_{11}^{m} = \varepsilon_{22}^{m} = 1 - \frac{\left(1-\varepsilon_{11}^{m0}\right)}{1-\varepsilon_{11}^{m0}\left(1-h_c^m/h\right)}, \tag{8b}$$

where h is the film thickness; h_c^p and h_c^m are the critical thickness for the formation of dislocation in the FE and FM phases, respectively;[19] and ε_{11}^{p0} and ε_{11}^{m0} are the corresponding pseudomorphic in-plane misfit strains, defined as follows:

$$\varepsilon_{11}^{p0} = \varepsilon_{22}^{p0} = \left(a_p - a_s\right)/a_p, \tag{9a}$$

$$\varepsilon_{11}^{m0} = \varepsilon_{22}^{m0} = \left(a_m - a_s\right)/a_m, \tag{9b}$$

where a_p and a_m are the in-plane parameters of the FE and FM phases, respectively, and a_s is the lattice parameter of the cubic substrate. The vertical epitaxial misfit strain is expressed as $\varepsilon_{33}^{t} = (1-\eta)\varepsilon_{33}^{p} + \eta\varepsilon_{33}^{m}$, where $\varepsilon_{33}^{p} = -\varepsilon_{33}^{m} = -0.8\%$ is adopted.[12,13] The virtual stress-free strain $\varepsilon_{ij}^{\text{virtual}}$ should be distributed only inside the vacuum region, and the equilibrium strain produces vanishing stress in the vacuum region, which automatically satisfies the free surface boundary conditions.

The dynamic evolution of the virtual stress-free strain and the polarization are described by the time-dependent Ginzburg–Landau equations

$$\frac{\partial \varepsilon_{ij}^{\text{virtual}}(\mathbf{r},t)}{\partial t} = -K\frac{\delta F}{\delta \varepsilon_{ij}^{\text{virtual}}(\mathbf{r},t)}, \tag{10}$$

$$\frac{\partial P_i(\mathbf{r},t)}{\partial t} = -L\frac{\delta F}{\delta P_i(\mathbf{r},t)}, \tag{11}$$

where K and L are kinetic coefficients.

The dynamic evolution of the magnetization is obtained by solving the Landau–Lifshitz–Gilbert equation using the Gauss–Seidel projection method:[20,21]

$$\left(1+\alpha^2\right)\frac{\partial \mathbf{M}}{\partial t} = -\gamma_0 \mathbf{M}\times\mathbf{H}_{\text{eff}} - \frac{\gamma_0\alpha}{M_s}\mathbf{M}\times\left(\mathbf{M}\times\mathbf{H}_{\text{eff}}\right), \tag{12}$$

where γ_0 is the gyromagnetic ratio, α is the damping constant, and $H_{\text{eff}} = -(1/\mu_0)(\partial F/\partial \mathbf{M})$ is the effective magnetic field.

III. SIMULATION PARAMETERS AND MATERIAL PROPERTIES

The three-dimensional simulation system is composed of $64\times64\times N_z$ discrete grids, where N_z grids encompass the vacuum layer, multiferroic nanocomposite thin film, and substrate. With reference to Fig. 1(b), the top 6 layers are assumed to be the vacuum region, the bottom 40 layers are assumed to be the substrate, and the layers in between simulate the multiferroic nanocomposite thin film. The periodic boundary conditions are applied along the x_1 and x_2 axes. The cell size in real space is chosen to be $l_0 = 1$ nm. The coefficients used in the simulation are listed below.[15]

For $BaTiO_3$,

$$\alpha_1 = 4.124(T-115)\times10^5 \text{C}^{-2}\text{m}^2\text{N}, \alpha_{11} = -2.097\times18^8\text{C}^{-4}\text{m}^6\text{N},$$

$$\alpha_{12} = 7.974\times18^8\text{C}^{-4}\text{m}^6\text{N}, \alpha_{111} = 1.294\times10^9\text{C}^{-6}\text{m}^{10}\text{N},$$

$$\alpha_{112} = -1.950\times10^9\text{C}^{-6}\text{m}^{10}\text{N}, \alpha_{123} = -2.500\times10^9\text{C}^{-6}\text{m}^{10}\text{N},$$

$$\alpha_{1111} = 3.863\times10^{10}\text{C}^{-8}\text{m}^{14}\text{N}, \alpha_{1112} = 2.529\times10^{10}\text{C}^{-8}\text{m}^{14}\text{N},$$

$$\alpha_{1122} = 1.637\times10^{10}\text{C}^{-8}\text{m}^{14}\text{N}, \alpha_{1123} = 1.367\times10^{10}\text{C}^{-8}\text{m}^{14}\text{N},$$

$$Q_{11} = 0.10\text{C}^{-2}\text{m}^4, Q_{12} = -0.034\text{C}^{-2}\text{m}^4, Q_{44} = 0.029\text{C}^{-2}\text{m}^4, T = 25^\circ\text{C},$$

$$c_{11} = 1.78\times10^{11}\text{Nm}^{-2}, c_{12} = 0.96\times10^{11}\text{Nm}^{-2}, c_{44} = 1.22\times10^{11}\text{Nm}^{-2}.$$

For $CoFe_2O_4$,

$$M_s = 4\times10^5\,\text{A/m}, \lambda_{100} = -590\times10^{-6}, \lambda_{111} = 120\times10^{-6}, K_1 = 3\times10^5\text{J/m}^3, K_2 = 0\,\text{J/m}^3,$$

$$A = 7\times10^{-12}\,\text{J/m}.$$

The in-plane lattice parameters for $BaTiO_3$ and $CoFe_2O_4$ are $a_p = 0.399$ nm and $a_m = 0.419$ nm, and the cubic parameters for the substrates $SrTiO_3$ and $DyScO_3$ are a_s ($SrTiO_3$) $= 0.3905$ nm and a_s ($DyScO_3$) $= 0.3943$ nm.[12,22] The critical thickness for the formation of dislocation is on the order of several nanometers. The values $h_c{}^p = h_c{}^m = 4$ nm are adopted in the present study. The volume fraction of $CoFe_2O_4$ is set as 35%. For simplicity, elastic homogeneity is assumed in the material whose elastic constants are taken as those of $BaTiO_3$. Considering the case where there is an in-plane compressive stress field in the ferroelectric phase, the initial polarization is set to be along the x_3 direction. Upon switching the direction of the applied magnetic field from the x_1 to the x_3 axis, the MIEP is given by $\Delta\bar{P}_3 = \bar{P}_3\,(\mathbf{H}//x_1) - \bar{P}_3\,(\mathbf{H}//x_3)$, where $\bar{P}_3$ is the average polarization of the nanocomposite film.

IV. RESULTS AND DISCUSSION

Figure 2 presents the variation of the MIEP with respect to the thickness of a nanocomposite film. In a multiferroic composite, the ME coupling is essentially due to the stress-mediated interaction between the ferromagnetic and ferroelectric phases. In the present study, the magnetostrictive properties of the nanocomposite significantly affect the MIEP. By rotating the applied magnetic field from the x_1 to the x_3 direction, the $CoFe_2O_4$ nanopillars with a negative magnetostrictive constant λ_{100} tend to contract in the x_3 direction and extend along the x_1 axis. Consequently, the neighboring $BaTiO_3$ phase is subject to both lateral and vertical contraction. Through the electrostrictive effects, the out-of-plane contraction reduces the polarization P_3 while the in-plane contraction enhances P_3. Thus, the MIEP is attributed to the result of the competition between the lateral and vertical elastic interactions. In the present case, the vertical elastic interaction is more significant, which leads to the decrease of the out-of-plane polarization of the film. With increasing film thickness, the influences from the vertical

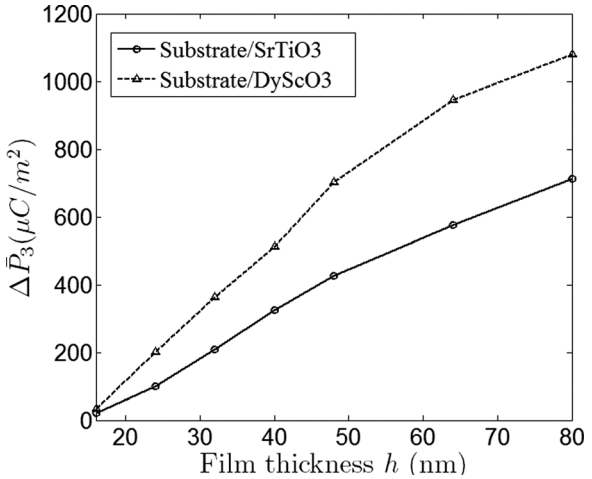

FIG. 2. The dependence of the magnetic-field-induced electric polarization on the film thickness.

elastic interaction would become more and more dominant. As a result, the magnitude of the MIEP increases with increasing film thickness. Moreover, in order to study the influence of the lateral interfacial strains, two substrates (i.e., $SiTiO_3$ and $DyScO_3$) are considered. With reference to Fig. 2, the MIEP is enhanced in the case of $DyScO_3$ due to the smaller lattice mismatch between the nanocomposite thin film and the substrate. Thus, one could infer that comparable lattice parameters of the substrate and the film are desirable in order to produce large magnetoelectric coupling effects.

Figure 3 presents the contours of the vertical stress σ_{33} with respect to the thickness of the film deposited on the $SrTiO_3$ substrate. It can be seen clearly from Fig. 3(a) that when the film thickness is small, the vertical stress is greatly influenced by the substrate and the free surface, which causes rapid variation of vertical stresses in the direction of the thickness. With reference to Figs. 3(b)–3(d), the influence of the vertical epitaxial strains on the vertical stress state is increased with increasing film thickness, which leads to a more homogeneously distributed vertical stress state along the direction of the thickness. Thus, it can be inferred that when the film is sufficiently thick, the influence of the substrate becomes negligible, and the vertical strains play an important role in manipulating the ME coupling effects. Consequently, the influence of the vertical strains on ME coupling effects cannot be neglected in the nanocomposite films in which large vertical strains would exist.

Recently, some experimental results[23] have illustrated that the vertical strain state could be controlled by tuning either the deposition frequency or the film composition. Thus, a coherent coefficient f is defined to describe the tunable vertical epitaxial strain, which is expressed as $\varepsilon_{33}{}^{t} = f[(1-\eta)\varepsilon_{33}^{p} + \eta\varepsilon_{33}^{m}]$. Note that $f=1$ stands for full coherence between the FE and FM phases, and $f=0$ denotes full relaxation of the lattice mismatch between the two phases. Figure 4 presents the relation between the MIEP and the coherent coefficient, which clearly shows that the MIEP can be enhanced by relaxing the vertical lattice mismatch. However, the small diameter of the nanopillars in the vertical heteroepitaxial nanocomposite thin film leads to little relaxation of the vertical strains in the film, which would greatly suppress the ME coupling effects. This may provide some clue as to why only weak ME coupling was observed in nanocomposite multiferroic films. It is worth noting that for thin films, the top and bottom electrodes should have some effect on the distribution of strains. However, for relatively thicker films, the influences from the electrodes as well as the substrate are not dominant, as demonstrated above.

In summary, the ME coupling effects in vertical heteroepitaxial nanocomposite thin films have been studied using the phase field method. It has been found that a better understanding of the ME coupling effects in such thin films can be achieved by incorporating the epitaxial strains in all three directions and the free surface and substrate effects. The MIEP is found to be strongly dependent on film thickness, as well as on vertical and lateral epitaxial strains.

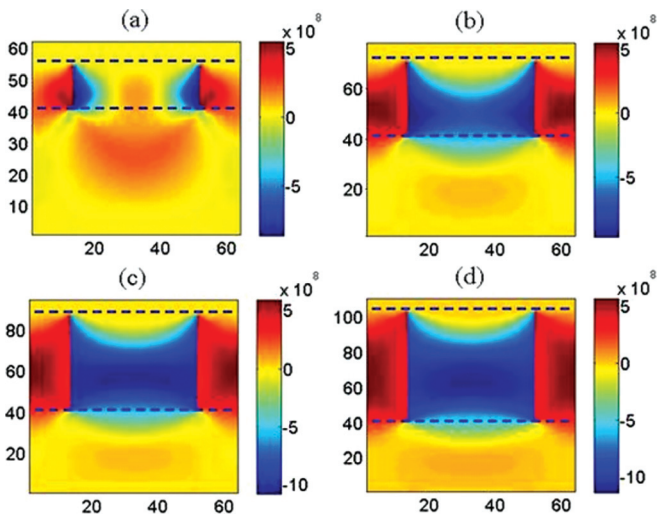

FIG. 3. (Color online) Variations of the vertical stress σ_{33} with the thickness of a film deposited on a $SrTiO_3$ substrate: (a) 16 nm, (b) 32 nm, (c) 48 nm, and (d) 64 nm.

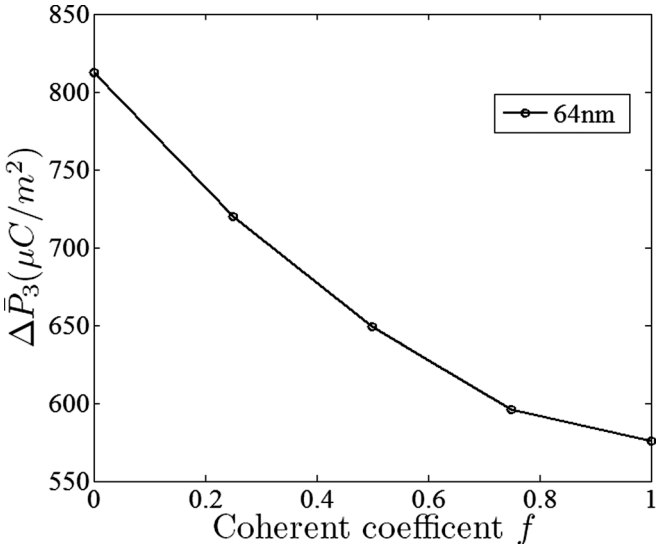

FIG. 4. Plot of the magnetic-field-induced electric polarization vs the coherent coefficient for the case of a film deposited on a $SrTiO_3$ substrate.

ACKNOWLEDGMENTS

Support from the Research Grants Council of the Hong Kong Special Administrative Region, China (Project Nos. HKU716508E and HKU716007E) is acknowledged.

[1]M. Fiebig, J. Phys. D **38**, R123 (2005).
[2]W. Eerenstein, N. D. Mathur, and J. F. Scott, Nature (London) **442**, 759 (2006).
[3]C. W. Nan, J. Appl. Phys. **103**, 031101 (2008).
[4]M. Gajek, M. Bibes, S. Fusil, K. Bouzehouane, J. Fontcuberta, A. Barthelemy, and A. Fert, Nature Mater. **6**, 296 (2007).
[5]J. F. Scott, Nature Mater. **6**, 256 (2007).
[6]M. Bibes and A. Barthelemy, Nature Mater. **7**, 425 (2008).
[7]T. Kimura, T. Goto, H. Shinani, K. Ishizaka, T. Arima, and Y. Tokura, Nature (London) **426**, 55 (2003).
[8]Y. Tokunaga, N. Furukawa, H. Sakai, Y. Taguchi, T. Arima, and Y. Tokura, Nature Mater. **8**, 558 (2009).
[9]J. Zhai, S. Dong, Z. Xing, J. Li, and D. Viehland, Appl. Phys. Lett. **89**, 083507 (2006).
[10]J. Ma, Z. Shi, and C. W. Nan, Adv. Mater. **19**, 2571 (2007).
[11]M. K. Lee, T. K. Nath, C. B. Eom, M. C. Smoak, and F. Tsui, Appl. Phys. Lett. **77**, 3547 (2000).
[12]H. Zheng, J. Wang, S. E. Lofland, Z. Ma, L. Mohaddes-Ardabili, T. Zhao, L. Salamanca-Riba, S. R. Shinde, S. B. Ogale, F. Bai, D. Viehland, Y. Jia, D. G. Gchlom, M. Wuttig, A. Roytburd, and R. Ramesh, Science **303**, 661 (2004).
[13]C. W. Nan, G. Liu, Y. H. Lin, and H. Chen, Phys. Rev. Lett. **94**, 197203 (2005).
[14]C. G. Zhong, Q. Jiang, and J. H. Fang, J. Appl. Phys. **106**, 014902 (2009).
[15]J. X. Zhang, Y. L. Li, D. G. Schlom, L. Q. Chen, F. Zavaliche, R. Ramesh, and Q. X. Jia, Appl. Phys. Lett. **90**, 052909 (2007).
[16]J. L. MacManus-Driscoll, P. Zerrer, H. Wang, H. Yang, J. Yoon, A. Fouchet, R. Yu. M. G. Blamire, and Q. X. Jia, Nature Mater. **7**, 314 (2008).
[17]Y. U. Wang, Y. M. Jin, and A. G. Khachaturyan, Acta Mater. **51**, 4209 (2003).
[18]Q. Y. Qiu, S. P. Alpay, and V. Nagarajan, J. Appl. Phys. **107**, 114105 (2010).
[19]J. S. Speck and W. Pompe, J. Appl. Phys. **76**, 466 (1994).
[20]X. P. Wang and C. J. Garcia-Cervera, J. Comput. Phys. **171**, 357 (2001).
[21]J. X. Zhang and L. Q. Chen, Acta. Mater. **53**, 2845 (2005).
[22]K. J. Choi, M. Biegalski, Y. L. Li, A. Sharan, J. Schubert, R. Uecker, P. Reiche, Y. B. Chen, X. Q. Pan, V. Gopalan, L. Q. Chen, D. G. Schlom, and C. B. Eom, Science **306**, 1005 (2004).
[23]Z. X. Bi, J. H. Lee, H. Yang, Q. X. Jia, J. L. MacManus-Driscoll, and H. Y. Wang, J. Appl. Phys. **106**, 094309 (2009).